

Optimal Continuous- to Discrete-Variable Bipartite Entanglement Conversion

Pak-Tik Fong,* Ruchir Tullu, and Hoi-Kwan Lau

*Department of Physics, Simon Fraser University,
Burnaby, British Columbia V5A 1S6, Canada*

(Dated: March 16, 2026)

Discrete-variable (DV) entanglement is crucial for numerous quantum applications, yet its deterministic generation in many bosonic systems remains experimentally challenging. In contrast, continuous-variable (CV) entanglement can be produced efficiently. We propose two optimal schemes for converting CV bipartite entanglement into DV entanglement using only local operations and classical communication. The first scheme extracts maximally entangled qubit pairs at the theoretically maximal rate, while the second probabilistically produces a maximally entangled qudit pair with the highest average entanglement. In both schemes, we quantify the optimal performance and identify the measurement operators required for implementation. Notably, using only a sequence of binary measurements, our approach can succeed in a finite number of measurement rounds on average, even though the CV resource is infinite-dimensional. Our schemes improve the feasibility of implementing DV-based quantum technologies on bosonic platforms.

I. INTRODUCTION

A wide range of quantum technologies, including quantum communication [1–3], quantum sensing [4] and quantum computing [5], are based on discrete-variable (DV) units, like qubits. Since only a small number of basis states is required in each degree of freedom, DV technologies can be implemented with a wide range of quantum systems that contain only a few controllable and stable states, such as defect centers [6]. However, these technologies are also occasionally implemented with bosonic systems, in which each degree of freedom (mode) exhibits effectively infinite levels. For example, microwave resonators can be a robust host of quantum information in circuit quantum electrodynamics (QED) architecture [7, 8], and the high mobility of photons makes them the dominant carriers of information in quantum communication [9–11].

While DV entanglement, in the form of maximally entangled qubits or qudits, is an essential resource for nearly all quantum technologies, their direct generation on bosonic platforms is usually not trivial. For example, generating photonic DV entanglement usually relies on probabilistic processes [12–15] or requires strong nonlinearities [16]. By contrast, continuous-variable (CV) Gaussian entanglement can be generated deterministically by quadratic (in mode operators) interaction, which is readily realizable in most bosonic platforms [17–26].

Nevertheless, maximal CV entanglement is unattainable because it involves infinite energy. Directly applying realistic but non-maximal CV entanglement in quantum technologies introduces un-

wanted noise [27–30]. Furthermore, far fewer quantum technologies have been developed for CV quantum information compared with their DV counterparts. These limitations reduce the practical utility of CV entanglement. Converting Gaussian CV entanglement into DV entanglement therefore provides a possible route to resolve this limitation [31–38].

CV-to-DV entanglement conversion has been extensively implemented in optical systems. The most notable example is the maximal qubit entanglement generated via spontaneous parametric down-conversion (SPDC); it is the entangled single-photon qubit states post-selected from a Gaussian photonic state that is generated by quadratic interaction [31–34]. Various improvements to the DV entangled photon source have also been considered by using photon addition, subtraction [35, 39], and noiseless linear amplification (NLA) [40]. In hybrid platforms, where both physical qubits and bosonic modes are available, entanglement can be transferred from modes to qubits by interaction and measurement [37, 38, 41]. Nevertheless, the efficiency of these schemes strongly depends on the interactions available in each platform. The fundamental optimality of CV-to-DV entanglement conversion remains unclear.

In this work, we address this question using the framework of entanglement transformation [42, 43], which considers the conversion of a single bipartite entangled state into another through local operations and classical communication (LOCC). Our aim is to study the optimal performance of generating maximal DV entanglement from a single copy of two-mode-squeezed vacuum (TMSV) state, which is local unitarily equivalent to any two-mode entangled Gaussian pure state [44]. We note that this framework is distinct from entanglement distillation [45, 46], which aims to extract a collection of maxi-

* Email: ptf@sfu.ca

maximally entangled states from many weakly entangled copies.

We find that the conversion can be considered optimal in two different and incompatible ways, as illustrated in Fig. 1. The first type of optimality aims to achieve the highest possible successful rate of generating a maximally entangled qubit pair. We show that the generation is deterministic whenever the squeezing strength of the TMSV exceeds 7.66 dB. Below this threshold, we discover the relation between squeezing and maximum conversion probability, and find that none of the existing schemes achieves the theoretical optimum. We identify the positive operator-valued measures (POVMs) by using Hardy's method of areas [47], which requires at least quadratically fewer POVMs than other known methods [42, 48]. The second type of conversion aims to produce a maximally entangled qudit pair where the dimension d is randomly determined; it is optimal when the average converted entanglement is maximum [47]. We also identify the relation between the amounts of converted entanglement and squeezing, as well as the implementing POVMs.

Because most physical measurement is binary in outcomes, we propose a binary search [49] method to use a sequence of binary measurements to implement the conversion POVMs. Remarkably, we find that the conversion can be accomplished in a finite number of binary measurement rounds on average, even though the CV system is infinite dimensional. We also discuss a possible implementation of the measurements in realistic hybrid qubit-oscillator platforms.

This paper is organized as follows. In Sec. II, we first review the general framework of the entanglement transformation. Then, in Sec. III, we present the optimal conversion scheme for the first scenario, obtaining a maximally entangled qubit pair with the highest probability. In Sec. IV, we extend the techniques for the second scenario, achieving the highest average entanglement in the qudits converted. Sec. V discusses the binary search strategy and its efficiency. Then, we discuss the physical implementations of the binary measurements in Sec. VI. Finally, we conclude our work in Sec. VII.

II. ENTANGLEMENT TRANSFORMATION

We begin by reviewing the framework of the entanglement transformation [42, 46]. Suppose that two parties, Alice and Bob, share an initial entangled state

$$|\Psi_\alpha\rangle = \sum_{n=0}^{\infty} \sqrt{\alpha_n} |u_n\rangle_A |v_n\rangle_B, \quad (1)$$

with the Schmidt coefficients $\sqrt{\alpha_n}$. Here, the Schmidt coefficients are arranged in descending order, i.e. $\alpha_n \geq \alpha_{n+1}$. $\{|u_n\rangle_A\}$ and $\{|v_n\rangle_B\}$ are the Schmidt bases of Alice's and Bob's systems respectively. Our task is to transform this state into a target state that the Schmidt coefficients are given by $\sqrt{\beta_n}$, i.e.

$$|\Psi_\beta\rangle = \sum_{n=0}^{\infty} \sqrt{\beta_n} |\tilde{u}_n\rangle_A |\tilde{v}_n\rangle_B, \quad (2)$$

where $\{|\tilde{u}_n\rangle_A\}$ and $\{|\tilde{v}_n\rangle_B\}$ are the new Schmidt bases which can be transformed from the original ones via local unitaries.

As discovered by Nielsen [42], a deterministic transformation via LOCC is possible if and only if the squared Schmidt coefficients of the target state majorize those of the initial state, i.e.

$$\sum_{n=l}^{\infty} \alpha_n \geq \sum_{n=l}^{\infty} \beta_n, \quad (3)$$

for all integer $l \in [0, \infty)$. While this condition implies that the target state cannot have more entanglement than the initial state, we note that the amount of entanglement is not the only factor that determines the possibility of deterministic transformation. It is also determined by the detailed distribution of the Schmidt coefficients [50].

When the majorization condition (3) is not satisfied, the transformation cannot be performed deterministically but only probabilistically. Vidal showed that the maximum success probability is determined by the minimum ratio of the cumulative probabilities [43], i.e.

$$P_{\max} = \min_{l \in [0, \infty)} \frac{\sum_{n=l}^{\infty} \alpha_n}{\sum_{n=l}^{\infty} \beta_n}. \quad (4)$$

III. CONVERTING TMSV TO MAXIMALLY ENTANGLED QUBIT PAIR

TMSV states can be generated from vacuum by using parametric amplification interaction that is widely available in bosonic platforms [17–25]. It is also known that any pure two-mode Gaussian state, which is the CV state that can be produced from vacuum by applying general quadratic interaction, can be transformed to TMSV by using only local Gaussian unitaries [44]. TMSV states have wide utilities in CV quantum technologies because it exhibits quantum correlations between the continuous quadratures of two modes, i.e. the correlated fluctuations of q -quadratures and anti-correlated fluctuations of p -quadratures are both below the shot-noise

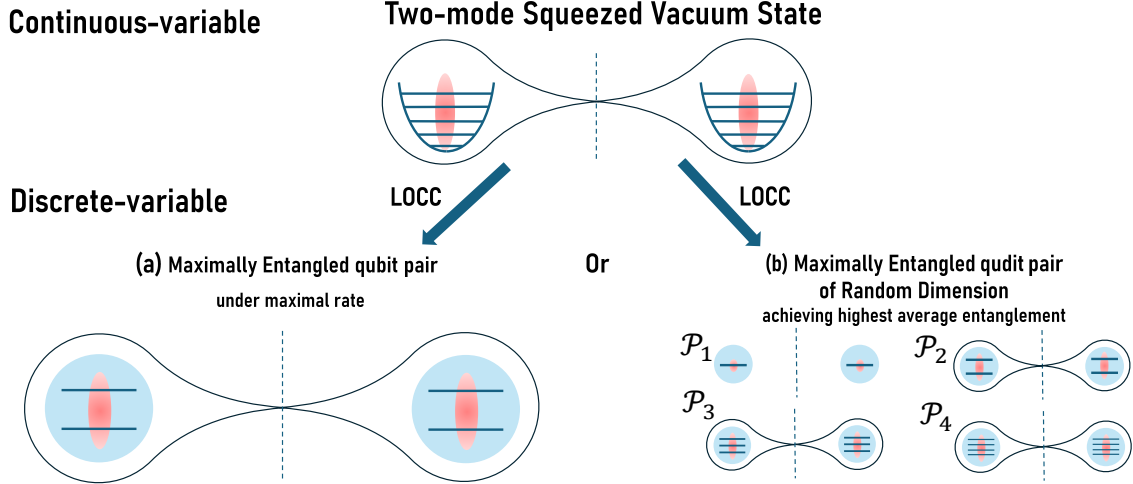


FIG. 1. Illustration of CV-to-DV entanglement conversion by transforming a TMSV state into a maximally entangled qudit pair via LOCC. (a) The first scenario considers transforming a TMSV state into a maximally entangled qubit pair with the highest possible rate. (b) In the second scenario, a TMSV is transformed into a maximally entangled qudit pair with random dimension d . \mathcal{P}_d is the probability of getting a qudit pair with dimension d . The scheme is optimal when the set of probabilities $\{\mathcal{P}_d\}$ gives the average entanglement is the highest.

limit, $\langle(\hat{q}_A - \hat{q}_B)^2\rangle = \langle(\hat{p}_A + \hat{p}_B)^2\rangle = e^{-2r} < 1$. Here \hat{q} and \hat{p} are respectively the q - and p -quadrature operators; subscripts A and B denote the modes of Alice and Bob respectively; r is the squeezing parameter. The infinitely squeezed TMSV state, i.e. $r \rightarrow \infty$, is also known as Einstein-Podolsky-Rosen (EPR) state because it resembles the quantum state in the seminal thought experiment [51].

To study the CV-to-DV entanglement conversion, we express the TMSV state in Schmidt decomposition [18],

$$|\text{TMSV}\rangle = \sqrt{1 - \lambda^2} \sum_{n=0}^{\infty} \lambda^n |n\rangle_A |n\rangle_B, \quad (5)$$

where $\lambda \equiv \tanh r$ and $|n\rangle$ is the n -boson Fock state. The squared-Schmidt coefficients are given by

$$\alpha_n = (1 - \lambda^2)\lambda^{2n} \quad \text{for } n \in [0, \infty). \quad (6)$$

Our target is to obtain a maximally entangled qubit pair, i.e. the state with the squared-Schmidt coefficients

$$\beta_n \equiv \begin{cases} 1/2 & \text{for } n = 0, 1 \\ 0 & \text{otherwise} \end{cases}. \quad (7)$$

We note that the TMSV state possesses infinitely many nonzero Schmidt coefficients, whereas the DV maximally entangled qubit pair has only two.

A. Optimal Conversion Rate

By using the majorization condition (3), we find that a maximally entangled qubit pair can be deterministically converted from a TMSV only when $\lambda \geq 1/\sqrt{2}$, which corresponds to a squeezing strength greater than 7.66 dB. We refer to this as the *threshold squeezing* strength. Notably, the amount of entanglement possessed by a threshold TMSV is equal to 2 ebits. It shows that the possibility of entanglement transformation is not determined solely by the amount of entanglement contained in the initial and target states. Generally, there is a price to pay to obtain an entangled state with the desired structure, i.e. the desired distribution of Schmidt coefficients.

When the squeezing strength is below the threshold value, $\lambda < 1/\sqrt{2}$, the conversion cannot succeed with certainty. By using Eq. (4), we find that the maximum success probability is given by $2\lambda^2$. Therefore, the maximal success probability of the entanglement conversion is summarized as

$$P_{\max} = \min(1, 2\lambda^2). \quad (8)$$

As mentioned, CV-to-DV entanglement conversion plays a significant role in bosonic quantum technologies, so various implementations have been proposed for different platforms. It would be interesting to know how efficient the existing schemes are, when comparing to the theoretical maximum Eq. (8). We define the conversion rate as the success probability for obtaining one copy of maximally entangled qubit

pair per each TMSV state resource.

A widely used entangled photon source in linear quantum optics experiments is SPDC, in which a nonlinear crystal is pumped by a classical laser. The pump activates a parametric interaction that will generate a TMSV state [52] between a degree of freedom in the signal and another in the idler. The choice of degrees of freedom varies across implementations, they could be, e.g. time bins or polarizations [53]. Generally, the pump is weak in the sense that the state is dominated by the vacuum and single-photon-pair components. In experiments, two pairs of TMSV are usually generated in different degrees of freedom. As an example, we illustrate in Fig. 2 (a) the time-bin entanglement source, where two pump pulses are applied sequentially and produce a TMSV between each pair of early and late time bins [54, 55]. The total state is given by

$$\begin{aligned} |\text{TMSV}\rangle^{\otimes 2} &= |00\rangle_s |00\rangle_i \\ &+ \lambda |01\rangle_s |01\rangle_i + \lambda |10\rangle_s |10\rangle_i + O(\lambda^2), \end{aligned} \quad (9)$$

where the subscripts s and i respectively denote the signal and idler modes; the left and right indices in each ket respectively denote the photon number in the late and early time bins. Experiments usually proceed with Alice and Bob, respectively, collect the signal and idler modes, manipulate the collected modes, and subject them to photon detection. By post-selecting the events that both Alice and Bob record a single-photon click, the observations are originated from the equal superposition of early- and late-time photon pairs (i.e. second and third terms in Eq. (9)), which corresponds to a maximally entangled single-photon qubit pair [31, 56]. Overall, with perfect collection efficiency, SPDC photon source will generate a maximally entangled qubit pair from two TMSV.

Apart from SPDC, other optical protocols have been proposed to generate maximally entangled qubit pairs from TMSV through number-resolving detections [33], photon addition and/or subtraction [35, 39], and NLA [40]. For hybrid qubit-oscillator systems, entanglement between two qubits can be established through interacting with the entangled oscillators [37, 38]. A recent scheme suggests that entanglement can be downloaded from a two-mode CV cluster state, which can be converted from TMSV by local unitaries, to two physical qubits [41].

In Figs. 2 (b) and (c), we compare the conversion rates of these established methods with the theoretical optimum. We find that no known scheme is optimal in all range of squeezing. Special interest is given to the weak-squeezing regime that most optical schemes are operating at. The conversion

rate of the SPDC source [31, 54, 56] is found to be roughly half of P_{\max} when $\lambda \ll 1$ (see Appendix A for detailed calculation). The sub-optimality originates from the post-selection process based on photon measurement: it collapses the superposition, and thus breaks the entanglement, between vacuum and the non-zero-photon states. Nevertheless, given the severe restriction of linear optics, particularly all passive optical elements must preserve the photon number, the mere half performance deficient is surprisingly minor. For other optical schemes, we find that NLA [40] is almost optimal in the weak-squeezing regime (see Appendix A). It is because in this regime the NLA projector coincides with the dominant POVM in the optimal scheme, which we will discuss further in the next subsection. For hybrid systems, the conversion rate of the entanglement downloading [41] is low (see Appendix A). It is understandable because the scheme focuses on preserving the structure of many-body entanglement, while the two-body efficiency is not a priority.

B. POVMs for Optimal Scheme

To implement entanglement transformation, Nielsen [42, 46] suggests a protocol that involves sequential measurements and local transformation by both Alice and Bob. The method is later simplified by Hardy by using a "method of areas" [47] and by Jensen and Schack by using Birkhoff-von Neumann theorem [48]. These schemes can be characterized by the POVMs corresponding to all possible measurement outcomes obtained during the processes. Since measurement is the most time-consuming and noisy element in many physical platforms, we would like to reduce the number of measurements involved in a CV-to-DV entanglement conversion. It is thus interesting to know the number of POVMs required by each scheme; as will be discussed in Sec. V, the number of POVMs is related to the required rounds of binary measurement.

A TMSV state contains infinite Schmidt coefficients. In practice, we can only address a finite number of them, so we truncate the state in Eq. (5) to consider only the N largest Schmidt coefficients, i.e. up to $N - 1$ excitations in each mode. In Fig. 3, we compare the number of outcomes required in different CV-to-DV entanglement conversion schemes. We find that Nielsen's method [42, 46] almost always removes one Schmidt coefficient in each round of binary measurement, so the whole process takes $\mathcal{O}(N)$ rounds of measurement, which consists of $\mathcal{O}(2^N)$ measurement outcomes. Jensen and Schack's method [48] relies on decomposing the double-stochastic matrix that maps the vector

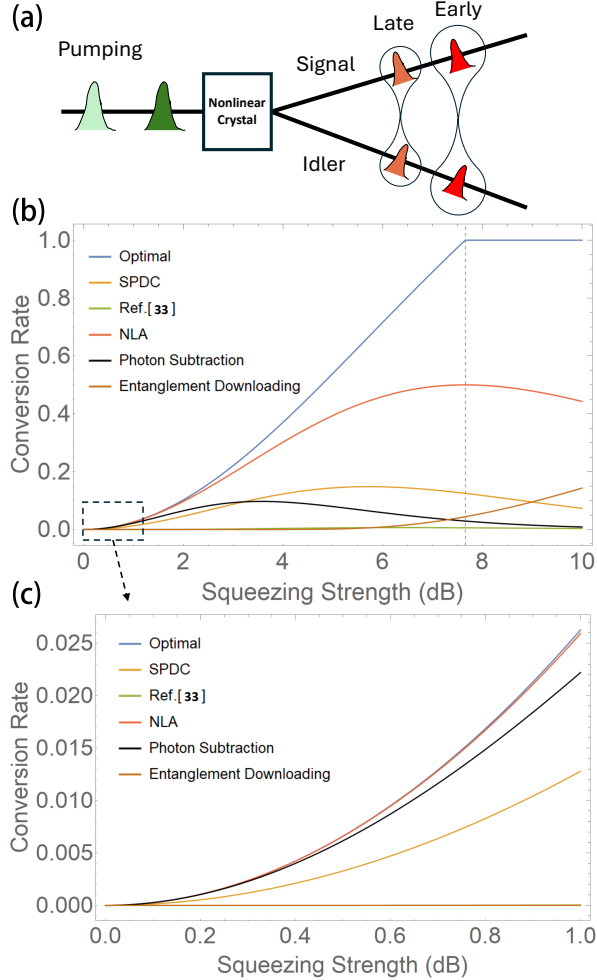


FIG. 2. (a) The illustration of the probabilistic generation of a maximally entangled single-photon time-bin qubit pair from the SPDC photon source. (b) The conversion rates of our optimal scheme and several existing schemes. The vertical gray-dashed line indicates the threshold squeezing strength. The dashed box indicates the weak-squeezing regime. (c) The zoom-in of the weak-squeezing regime.

$\{\beta_n\}$ to $\{\alpha_n\}$ into permutations. Since the double-stochastic matrix is N^2 in dimension and each permutation represents one POVM, there will be $\mathcal{O}(N^2)$ POVMs. Finally, by using Hardy’s method, we find that CV-to-DV conversion can be completed with only $\mathcal{O}(N)$ POVMs [47]. This represents at least quadratic reduction of POVMs when compared to other schemes. In the following, we illustrate the application of Hardy’s method in CV-to-DV conversion.

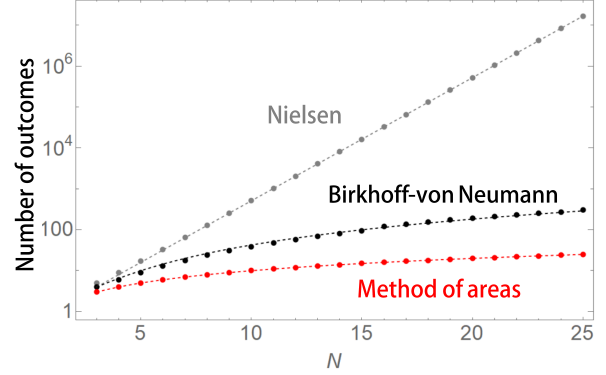


FIG. 3. The number of POVMs yielded by different entanglement transformation schemes against the boson number truncation N of a TMSV. The presented data corresponds to $\lambda = 0.5$, but the behavior is typical for other values of λ . The Nielsen’s scheme, Birkhoff-von Neumann’s algorithm and the method of areas require 2^{N-1} , $(N-1)^2/2 + 2$ and N POVMs, respectively.

C. Hardy’s Method of Areas

Hardy’s method of areas expresses the squared Schmidt coefficients as a column chart ordered by decreasing height, where each column is unit-width, painted with a distinct colour, and has an area equal to the corresponding Schmidt coefficient. As an example, Fig. 4 (a) shows the chart of a TMSV. Hardy showed that entanglement transformation is equivalent to dividing the columns into patches and stacking the patches onto the columns to the left [47]. If this process can form the chart of the target state, e.g. Fig. 4 (b) for a maximally entangled qubit pair, the scheme is deterministic. Otherwise, a transformed chart should be constructed to fit in a compressed version of the target chart. Exploiting all possible chart transformations, the one that fits in a least compressed target chart, e.g. Fig. 4 (c), deduces the maximum probability of successful transformation. The pattern of the transformed chart also determines the measurement operators that implement such transformation [47].

To generate a maximal entangled qubit pair, the target chart consists of two equal-height columns. The columns can be divided into segments, such that in each segment there is only one colour in each column. We indicated the segment boundaries by dashed lines in Fig. 4 (b) and (c). According to Hardy’s method, the colours of each segment tell the initial Schmidt states that will be involved in the target state after transformation, and the total area covered by the segments will be the probability of obtaining such outcome. In our case, because the Schmidt bases of TMSV are paired Fock states,

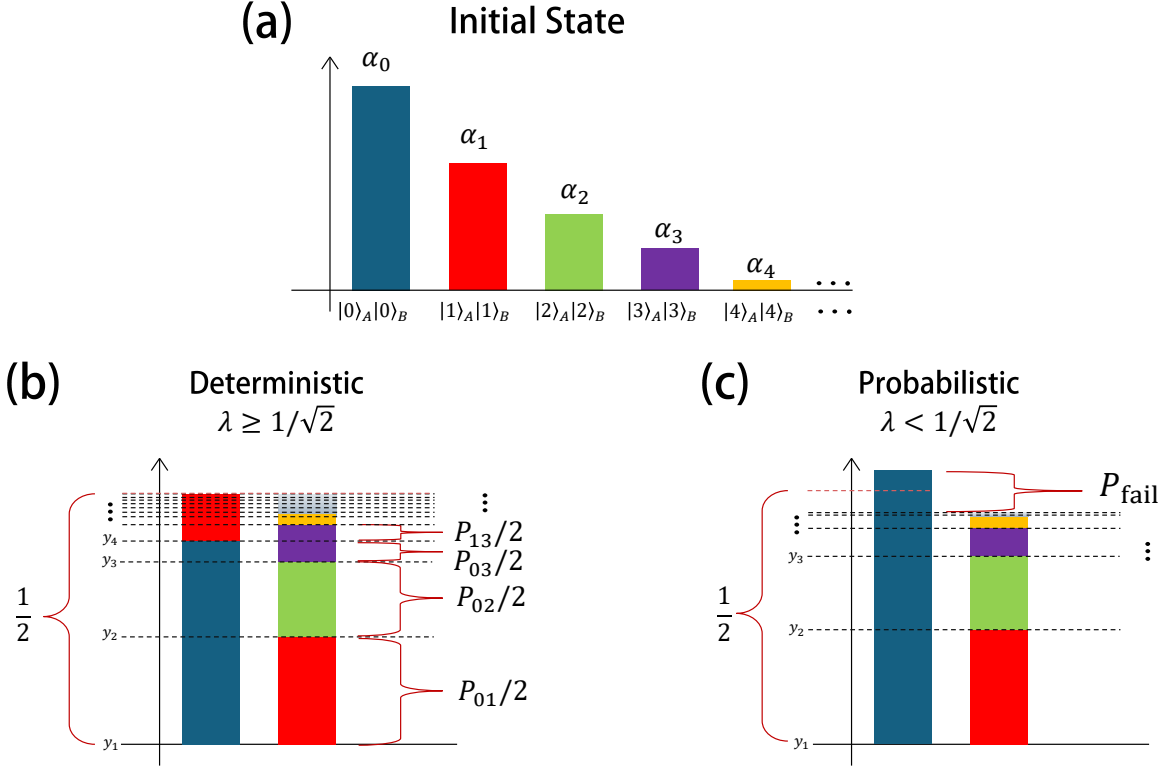


FIG. 4. Illustration of Hardy's method of areas. (a) The chart represents the initial TMSV state. Every column is painted in a different colour, and the area covered by each column is given by the squared Schmidt coefficients $\{\alpha_n\}$. (b) The transformed chart in the deterministic regime. The two columns have the same height $\beta_0 = \beta_1 = 1/2$, so the chart coincides with the target state. The boundaries of adjacent colours are labeled by $\{y_i\}$. The probability of obtaining $|\text{Bell}_{nm}\rangle$, P_{nm} , is determined by the area covered by the segment of columns between two adjacent boundaries, and the corresponding Fock states involved, $\{n, m\}$, are determined by the colours of the segment. (c) The transformed chart in the probabilistic regime. The heights of the first and second columns are respectively α_0 and $\sum_{n=1}^{\infty} \alpha_n$. Since $\alpha_0 > 1/2$, there is a segment consists of only the first but not the second column. This segment, whose height and covered area are both P_{fail} , corresponds to the failed conversion.

the target states will be equal superpositions of Fock states, i.e.

$$|\text{Bell}_{nm}\rangle = \frac{1}{\sqrt{2}} (|n\rangle_A |n\rangle_B + |m\rangle_A |m\rangle_B), \quad (10)$$

where $n \neq m$.

When the squeezing is above threshold, we can construct a transformed chart that consists of two columns with equal height as $1/2$, see Fig. 4 (b). Because it coincides with the target chart, the transformation is deterministic. When the squeezing is below threshold, the first initial column has height $1 - \lambda^2 > 1/2$, so it is higher than all the other columns combined. After transformation, the two columns thus have different height, so the conversion is not deterministic. Then there will be a segment in the first column that cannot pair with any patch in the second column. It corresponds to the failed conversion that the outcome becomes a separable state

$$|0\rangle_A |0\rangle_B.$$

The probability of getting a particular outcome is determined by the total area covered by the corresponding segments, which is the sum of the heights of the segments multiplied with the unit width. When $\lambda \geq 1/\sqrt{2}$, the deterministic regime, all segments are paired, so there is no failed conversion, i.e. the fail probability $P_{\text{fail}} = 1 - P_{\text{max}} = 0$. We note that in the deterministic regime there is no unique way to construct the transformed chart. For example, one can fill up the first column by using the patch cut from the second or any other columns. In this work, as illustrated in Fig. 4 (b), we consider a specific construction that fills the first transformed column with the patches from the first M initial columns, where the sum of areas covered by these columns is just larger than $1/2$, i.e. $\sum_{j=0}^{M-1} \alpha_j > 1/2 > \sum_{j=0}^{M-2} \alpha_j$. Then, the second transformed column consists of a patch of the M -th

initial column with height $1/2 - \sum_{j=0}^{M-1} \alpha_j$ and all the remaining initial columns. The segment boundaries are located at the colour boundaries of the first columns, $\{\alpha_n\}$ for $n < M - 1$, as well as those of the second columns, $\{\alpha_n - 1/2\}$ for $n \geq M - 1$. We rank them in ascending order, $\{y_0 = 0, y_1, y_2, y_3, \dots\}$. The probability of the l -th outcome will be given by $2(y_l - y_{l-1})$ for $l \in [1, \infty)$, and the corresponding Fock states involved in that outcome can be deduced from the colours of columns between the boundaries y_l and y_{l-1} .

For $\lambda < 1/\sqrt{2}$, the probabilistic regime, the fail probability P_{fail} is non-zero and given by the height of that unpaired part. It can be minimized by forming the first transformed column with only the first column of the initial chart, while the second transformed column consists of all the remaining initial columns, as illustrated in Fig. 4 (c). This is the unique construction of the transformed chart, because moving any patch to the first column will only reduce the transformation successful probability. The fail probability can be easily found as $P_{\text{fail}} = 1 - P_{\text{max}} = 1 - 2\lambda^2$. In this case, the boundaries of segments are simply given by $y_l = \sum_{j=1}^l \alpha_j$ for $l \in [1, \infty)$. The segment between the boundaries y_l and y_{l-1} corresponds to the $|0\rangle_A |0\rangle_B$ for the first column and $|l\rangle_A |l\rangle_B$ for the second column. Hence, the outcomes are $|\text{Bell}_{0l}\rangle$ and the corresponding probabilities are given by $P_{0l} = 2\lambda^{2l}(1 - \lambda^2)$ for $l \geq 1$.

Implementing the entanglement transformation deduced from Hardy's method requires only local measurements on one party, which we assumed to be Alice without loss of generality. The corresponding measurement operators \hat{M}_{nm} and \hat{M}_{fail} should respectively project the TMSV to the target states, $|\text{Bell}_{nm}\rangle$ and $|0\rangle_A |0\rangle_B$, with the probabilities P_{nm} and P_{fail} specified by the Hardy's method, i.e.

$$\begin{aligned} \hat{M}_{nm} |\text{TMSV}\rangle &= \sqrt{P_{nm}} |\text{Bell}_{nm}\rangle, \\ \hat{M}_{\text{fail}} |\text{TMSV}\rangle &= \sqrt{P_{\text{fail}}} |0\rangle_A |0\rangle_B. \end{aligned} \quad (11)$$

They can be easily found as

$$\begin{aligned} \hat{M}_{nm} &= \sqrt{\frac{P_{nm}}{2(1 - \lambda^2)}} \\ &\times (\lambda^{-2n} |n\rangle_A \langle n| + \lambda^{-2m} |m\rangle_A \langle m|), \\ \hat{M}_{\text{fail}} &= \sqrt{\frac{P_{\text{fail}}}{1 - \lambda^2}} |0\rangle_A \langle 0|, \end{aligned} \quad (12)$$

which are diagonal in the Fock basis. It is easy to check that these POVMs form a complete set in both

deterministic and probabilistic regimes, i.e.

$$\hat{M}_{\text{fail}}^\dagger \hat{M}_{\text{fail}} + \sum_{n=0}^{\infty} \sum_{m=0}^{\infty} \hat{M}_{nm}^\dagger \hat{M}_{nm} = \sum_{n=0}^{\infty} |n\rangle_A \langle n|. \quad (13)$$

The measurement corresponding to these POVMs can be realized by a single measurement process that has infinite outcomes [48], but this is usually difficult to implement in practice. Alternatively, we will discuss in Sec. V a measurement scheme that requires only a sequence of binary measurements.

IV. CONVERTING TMSV TO MAXIMALLY ENTANGLED QUDIT PAIR WITH RANDOM DIMENSION

Entanglement of a TMSV state increases with squeezing, so it is expected that more DV entanglement can be extracted from a stronger squeezed TMSV state. However, the average number of maximally entangled qubit pairs obtained from a TMSV plateaus at 7.66 dB. One could straightforwardly extend the entanglement transformation to create maximally entangled qudit pairs, i.e. the state with the squared-Schmidt coefficients

$$\beta_n = \begin{cases} 1/d & \text{for } n = 0, 1, \dots, d-1 \\ 0 & \text{otherwise} \end{cases}, \quad (14)$$

but such schemes will also plateau when the squeezing is sufficiently high that the transformation becomes deterministic. Nevertheless, maximal DV entanglement can also be obtained in other forms: entanglement concentration protocol is known to convert any bipartite entangled state to a maximally entangled qudit pair, where the dimension d is random [45, 57]. The probabilities \mathcal{P}_d of obtaining each d -dimensional entangled qudit pair depend on the local operations. For the optimal scheme that generates the highest average entanglement, the probabilities are known to be $\mathcal{P}_d = d(\alpha_{d-1} - \alpha_d)$ [47]. For CV-to-DV entanglement conversion, it is given by

$$\mathcal{P}_d = d\lambda^{2d-2}(1 - \lambda^2)^2. \quad (15)$$

The resulting average entanglement is

$$\begin{aligned} S_{\text{avg}} &= \sum_{d=1}^{\infty} \mathcal{P}_d S_d \\ &= -\frac{(1 - \lambda^2)^2}{\lambda^2 \ln 2} \frac{\partial \text{Li}_s(\lambda^2)}{\partial s} \Big|_{s=-1}, \end{aligned} \quad (16)$$

where $S_d = \log_2 d$ is the entanglement entropy of the d -dimensional maximally entangled qudit pair [58] and $\text{Li}_s(z)$ is a polylogarithm of order s [59].

The composition of the obtained entangled qudit pair, and hence the corresponding POVMs, can be learned from the method of areas, as illustrated in Fig. 5. Hardy found that the maximum average entanglement is obtained without transforming the chart. In this situation, the segment boundaries will be given by the heights of all columns, i.e. $\{\alpha_n\}$. The maximally entangled DV state of dimension d is specified by the segment that involves d columns, which is located between the boundaries at α_{d-1} and α_d . The entangled qudit pair obtained will be an equal superposition of the first d components in the Schmidt decomposition, i.e. the equal superposition of the first d Fock states in both modes,

$$|\varphi_d\rangle = \frac{1}{\sqrt{d}} \sum_{n=0}^{d-1} |n\rangle_A |n\rangle_B. \quad (17)$$

Considering the above state can be generated by the POVM $\hat{\mathcal{M}}_d$,

$$\hat{\mathcal{M}}_d |\text{TMSV}_\lambda\rangle = \sqrt{\mathcal{P}_d} |\varphi_d\rangle, \quad (18)$$

the measurement operators can be found as

$$\hat{\mathcal{M}}_d \equiv \lambda^{d-1} \sqrt{1 - \lambda^2} \sum_{n=0}^{d-1} \lambda^{-n} |n\rangle_A \langle n|, \quad (19)$$

for $d = 1, 2, \dots, \infty$. They satisfy the completeness condition $\sum_{d=1}^{\infty} \hat{\mathcal{M}}_d^\dagger \hat{\mathcal{M}}_d = \hat{I}$.

In Fig. 6, we compare the entanglement entropy of a TMSV state with the average DV entanglement obtained under the optimal schemes in Secs. III and IV. The entanglement generated by the random qudit scheme increases monotonically with the squeezing strength, in stark contrast to the maximal qubit scheme that saturates. Moreover, as squeezing increases, the gap between the entanglement of the initial TMSV state and the average DV entanglement obtained from the optimal random qudit scheme approaches a constant value, $\gamma/\ln(2) \approx 0.832746$, where γ is the Euler–Mascheroni constant [60].

V. REALIZING POVMs BY BINARY SEARCH

Since the measurement in most quantum platforms is binary, instead of implementing a many-outcome measurement [61], we propose to realize the POVMs by binary search, i.e. a sequence of binary measurements [49, 62].

For convenience, hereafter, we will relabel the required POVMs and the corresponding outcomes for any scheme as $\{\hat{E}_1, \hat{E}_2, \dots, \hat{E}_\infty\}$ and $\{E_1, E_2, \dots, E_\infty\}$ respectively; the POVMs are arranged in descending order of the probabilities, i.e. $P(E_1) \geq P(E_2) \geq \dots \geq P(E_\infty)$.

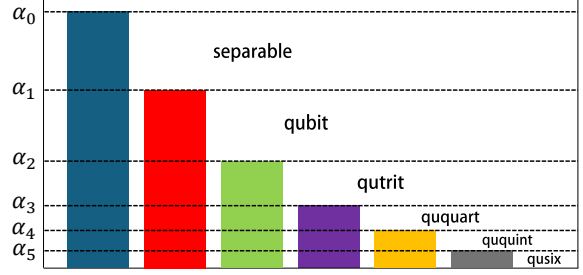


FIG. 5. Illustration of the method of areas for the optimal random qudit scheme. The segment boundaries (dashed) are located at the heights of the columns. The probability of obtaining a qudit pair with dimension d is given by the total area of columns between boundaries at α_{d-1} and α_d , and the corresponding Fock states involved are determined by the columns included in that segment.

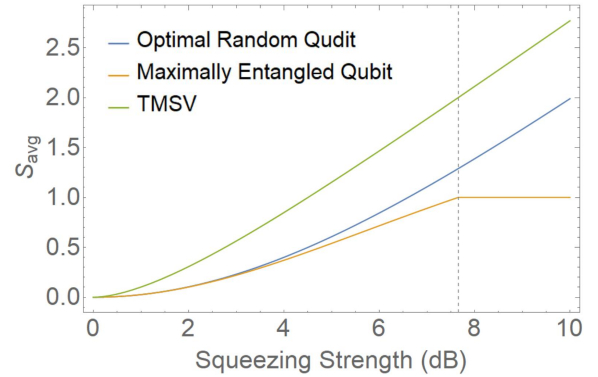


FIG. 6. Entanglement of the original TMSV state and the converted maximally entangled DV states versus squeezing strength.

A. One-Outcome-per-Round Binary Search

A straightforward implementation is to distinguish one outcome in each round of measurement. In this scheme, the binary POVMs implemented in the m -th round are

$$\{\hat{E}_m/\sqrt{F_m}, \sqrt{\hat{I} - \hat{E}_m^\dagger \hat{E}_m/F_m}\}, \quad (20)$$

where $F_m = \sum_{i=m}^{\infty} P(E_i)$ is the probability of failing to distinguish an outcome in the previous $m - 1$ rounds of measurement; \hat{I} is the identity operator. We illustrate the idea with a binary tree in Fig. 7 (a). The binary measurements are performed sequentially until an outcome is distinguished.

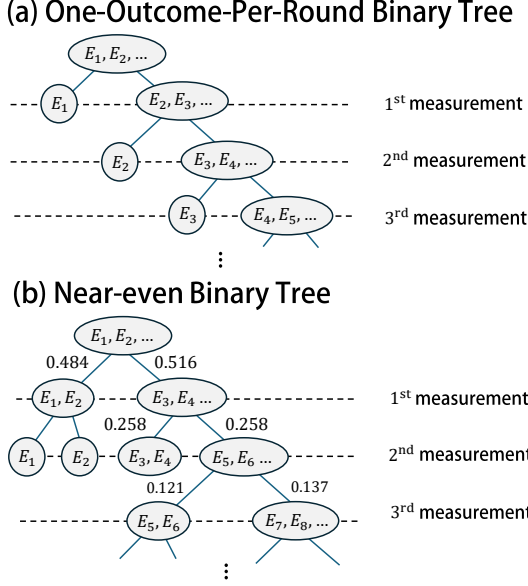


FIG. 7. Illustration of binary search trees. (a) The simple one-outcome-per-round binary search, which determines only one outcome in each round of binary measurement. (b) The near-even binary search for the case of $\lambda = 0.8$. In each round of binary measurement, the outcomes are divided into two groups according to Eq. (21). The probabilities of the binary outcomes are labeled beside the branches connecting the corresponding group.

B. Near-Even Binary Search

The above one-outcome-per-round (Sec. V A) scheme is not the only way to construct a binary tree; alternative construction can further reduce the measurement rounds. We propose a near-even binary search, illustrated in Fig. 7 (b), in which the two binary outcomes at each round are chosen to have probabilities as close as possible.

Our intuition is that our task of distinguishing a particular outcome is equivalent to revealing the identity E_m of a random variable that follows the probability $P(E_m)$. Every binary measurement will provide us less than or equal to 1 bit of information about the random variable, and the amount of information is higher when the probabilities of the two outcomes are closer to each other. Therefore, by grouping the possible outcomes into two sets that have close probabilities in every binary measurement, we increase the information gained about the random variable in each round, thus reducing the required number of measurement rounds.

Nevertheless, grouping numbers into two sets that have minimal sum difference is known to be a hard problem [63]. Here we aim to use only a simple routine to reduce the probability difference between two

groups of outcomes, instead of looking for a grouping that minimizes the difference. Considering a task that aims to distinguish an outcome from M possible ones $\{E_1, \dots, E_M\}$. We divide them into two groups $B_0 = \{E_1, \dots, E_Y\}$ and $B_1 = \{E_{Y+1}, \dots, E_M\}$, where Y is the largest number that the first group has less total probability than the second, i.e.

$$\sum_{m=1}^{Y+1} P(E_i) > \sum_{m=1}^M P(E_i)/2 \geq \sum_{m=1}^Y P(E_i). \quad (21)$$

A binary measurement can be constructed with measurement operators \hat{B}_0 and \hat{B}_1 , which are determined by

$$\hat{B}_0^\dagger \hat{B}_0 = \mathcal{N} \sum_{m=1}^Y \hat{E}_m^\dagger \hat{E}_m, \quad (22)$$

with the normalization

$$\mathcal{N}^{-1} = \sum_{m=1}^M P(E_m), \quad (23)$$

and

$$\hat{B}_1^\dagger \hat{B}_1 = \hat{I} - \hat{B}_0^\dagger \hat{B}_0. \quad (24)$$

Since our POVMs for CV-to-DV entanglement conversion are diagonal in Fock basis, the binary measurement operators will also be Fock diagonal. If B_0 is obtained, the outcome belongs to one in the first group, otherwise the outcome belongs to the second. After the binary measurement, the number of outcomes need to be distinguished are reduced. The process continues until a specific outcome is identified.

In Fig. 7 (b), we demonstrate the group division method with the entanglement transformation of a TMSV with $\lambda = 0.8$ to a maximally entangled qubit pair. In descending order of probabilities, the corresponding POVMs of the first few outcomes are $\hat{E}_1 = \hat{M}_{02}, \hat{E}_2 = \hat{M}_{03}, \hat{E}_3 = \hat{M}_{01}, \hat{E}_4 = \hat{M}_{15}, \hat{E}_5 = \hat{M}_{14}, \hat{E}_6 = \hat{M}_{04}$ and their probabilities are $P(E_1) = P_{02} = 0.295, P(E_2) = P_{03} = 0.188, P(E_3) = P_{01} = 0.181, P(E_4) = P_{15} = 0.0773, P(E_5) = P_{14} = 0.0652, P(E_6) = P_{04} = 0.0555$ respectively. In the first round of division, the first two events $\{E_1, E_2\}$ are assigned to the binary outcome B_0 , such that their probabilities sum, labeled beside the branches in Fig. 7 (b), satisfies Eq. (21). The remaining outcomes, $\{E_3, E_4, \dots\}$, are assigned to binary outcome B_1 . If the first binary measurement gives B_0 , the next round of binary measurement will distinguish the outcome E_1 from E_2 . Otherwise, we divide the remaining outcomes into two groups, which in this case are $\{E_3, E_4\}$ and $\{E_5, E_6, \dots\}$. The process continues until we obtain a binary measurement outcome that contains only one outcome E_m .

C. Efficiency of Binary Search

We assess the efficiency of the binary search schemes by considering the average number of measurement rounds needed to obtain a ebit of maximal DV entanglement from a TMSV state,

$$\eta \equiv \langle R \rangle / S. \quad (25)$$

Here, the denominator S is the average amount of maximal DV entanglement, in the unit of ebit, obtained per entanglement transformation. For the maximal qubit scheme in Sec. III, S will be the successful probability, $S = P_{\max}$. For the random qudit scheme in Sec. IV, S will be the average obtained entanglement in Eq. (16), $S = S_{avg}$. The numerator is the expected number of measurement rounds for the entanglement transformation to complete, $\langle R \rangle = \sum_{n=1}^{\infty} P(E_n)R(E_n)$, where $R(E_m)$ denotes the number of measurement rounds required to distinguish the outcome E_m .

To appraise the performance of our binary search method, we consider a lower bound of binary measurement rounds that is necessary but might not always be attainable. Our idea is to treat the measurement sequence as a process to reveal the identity of a random variable that has the identities E_m with probability $P(E_m)$. The minimum information required to describe this variable is thus given by the Shannon entropy $H = \sum_{n=1}^{\infty} P(E_n) [-\log_2 P(E_n)]$ [46]. Because each round of binary measurement can at most reveal 1 bit of information, we can draw a lower bound of measurement round as $\langle R \rangle \geq H$. Since our near-even scheme attempts to increase the information revealed in each round by making the binary outcomes more evenly probable, we expect the performance of our scheme will be closer to the bound than the simple one-outcome-per-round scheme.

Fig. 8 (a) compares the efficiencies for the maximal qubit scenario in Sec. III. In the probabilistic regime, i.e. $\lambda < 1/\sqrt{2}$, both schemes coincide. It is because the probability of the L -th outcome, $P(E_L)$, is always larger than that of all the following outcomes combined, $\sum_{m=L+1}^{\infty} P(E_m)$, so in our scheme the binary outcome B_0 also contains only one outcome E_L . In the deterministic regime, on the other hand, our scheme performs much better than one-outcome-per-round and is close to the lower bound in a wide range of squeezing. Remarkably, at the threshold squeezing 7.66 dB, both schemes attain the lower bound. In this situation, a maximally entangled qubit pair can be obtained with two rounds of measurement on average, even though the original TMSV contains infinite non-zero Schmidt coefficients.

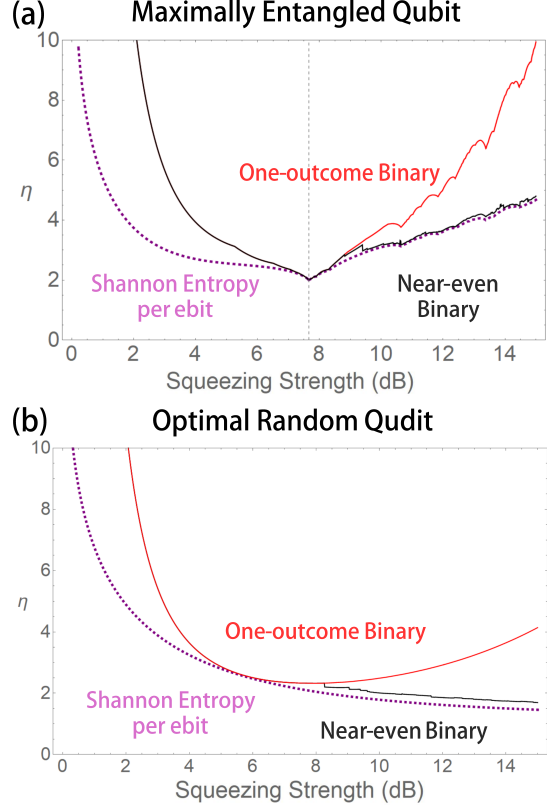


FIG. 8. Average number of binary measurement rounds required to obtain 1 ebit of maximal DV entanglement at different squeezing strength. Black and red curves respectively refer to the efficiencies of our near-even and the simple one-outcome-per-round schemes. The lower bound imposed by Shannon entropy is shown as purple dashed for comparison. (a) Schemes for obtaining a maximally entangled qubit pair. (b) Schemes for obtaining randomly a maximally entangled qudit pair.

For the random qudit scenario in Sec. IV, the efficiencies are shown in Fig. 8 (b). For squeezing strengths below 8 dB, two schemes coincide again because the binary outcome B_0 contains only one outcome in our scheme. At around 5.5 dB, both schemes can reach the lower bound imposed by Shannon entropy.

VI. PHYSICAL IMPLEMENTATION OF POVMS

To realize our schemes, Alice is required to implement the Fock-diagonal binary measurement opera-

tors

$$\begin{aligned}\hat{B}_0 &= \sum_{n=0}^{\infty} C_n |n\rangle_A \langle n|, \\ \hat{B}_1 &= \sum_{n=0}^{\infty} \sqrt{1 - C_n^2} |n\rangle_A \langle n|,\end{aligned}\quad (26)$$

where the coefficients C_n are determined by Eqs. (22) and (24). Here, we illustrate a possible physical implementation of the measurement operators (26) by coupling the bosonic mode to an ancillary qubit and then measuring the qubit.

We initialize the qubit in $|g\rangle$ and then apply the boson-number-dependent rotation

$$|n\rangle_A |g\rangle \rightarrow C_n |n\rangle_A |g\rangle + \sqrt{1 - C_n^2} |n\rangle_A |e\rangle, \quad (27)$$

where $|g\rangle$ and $|e\rangle$ are the qubit computational basis states. This transformation can be realized using a photon-number-selective qubit rotation (SQR) gate [64], $\hat{U}_{\text{SQR}} \equiv \sum_n \exp(-i\phi_n \hat{\sigma}_y) |n\rangle \langle n|$, where the rotation angles are $\phi_n = \arccos(C_n)$ and $\hat{\sigma}_y \equiv i |e\rangle \langle g| - i |g\rangle \langle e|$. Such SQR gates have been implemented extensively in circuit QED platforms using multi-tone drives, which each tone addresses a qubit frequency that is shifted by a specific boson number state [65, 66]. It can also be engineered by using quantum signal processing techniques in any hybrid qubit-oscillator platforms that exhibit dispersive or Jaynes–Cummings couplings [67].

Following the above transformation, the auxiliary qubit is then projectively measured in the computational basis. The measurement outcome $|g\rangle$ heralds the implementation of \hat{B}_0 , while the outcome $|e\rangle$ corresponds to \hat{B}_1 .

VII. CONCLUSION

We have developed optimal schemes for converting realistic CV bipartite entanglement into maximal DV entanglement. Two optimal scenarios were analyzed: (i) converting a TMSV state into a maximally entangled qubit pair at the theoretically maxi-

imum successful rate, and (ii) converting into a maximally entangled qudit pair with random dimension that maximizes the average entanglement. In the first scenario, we identified the relation between the maximum successful rate and the squeezing strength of TMSV, and found that none of the existing CV-to-DV entanglement conversion schemes is optimal. For the second scenario, we identified the optimal probabilities of obtaining each maximally entangled qudit pair and analytically found the entanglement sacrificed during the conversion.

For both scenarios, we constructed the measurement operators that realize the optimal schemes. Among known methods of entanglement conversion, we found that the method of areas can accomplish the task with the fewest number of POVMs. We further developed a binary tree scheme to reduce the number of rounds of binary measurement to implement the POVMs. Although the number of required POVMs is infinite, our schemes can accomplish the conversion in a finite number of measurement rounds on average. These techniques make CV-to-DV entanglement conversion experimentally feasible and resource-efficient.

Finally, we illustrated how the measurement operators can be implemented in hybrid qubit-oscillator platforms. Our work establishes a practical pathway to optimally generate broadly applicable DV entanglement from the efficiently produced CV entanglement. It opens new opportunities for hybrid quantum technologies that combine the advantages of both continuous- and discrete-variable quantum information, and facilitates the implementation of quantum technologies on physically advantageous bosonic platforms.

ACKNOWLEDGMENTS

This work is supported by the Natural Sciences and Engineering Research Council of Canada Discovery Grant (NSERC RGPIN-2021-02637), Alliance International Catalyst Quantum Grant (ALLRP 578638-22), and Canada Research Chairs (CRC-2020-00134). R. Tullu acknowledges support from an NSERC USRA.

-
- [1] N. Gisin and R. Thew, Quantum communication, *Nature Photonics* **1**, 165 (2007).
 - [2] A. K. Ekert, Quantum cryptography based on bell's theorem, *Phys. Rev. Lett.* **67**, 661 (1991).
 - [3] T. Jennewein, C. Simon, G. Weihs, H. Weinfurter, and A. Zeilinger, Quantum cryptography with entangled photons, *Phys. Rev. Lett.* **84**, 4729 (2000).

- [4] C. L. Degen, F. Reinhard, and P. Cappellaro, Quantum sensing, *Rev. Mod. Phys.* **89**, 035002 (2017).
- [5] D. Deutsch, Quantum theory, the church–turing principle and the universal quantum computer, *Proceedings of the Royal Society of London. A. Mathematical and Physical Sciences* **400**, 97 (1985).
- [6] R. Katsumi, K. Takada, F. Jelezko, and T. Yatsui,

- Recent progress in hybrid diamond photonics for quantum information processing and sensing, *Communications Engineering* **4**, 85 (2025).
- [7] A. Blais, R.-S. Huang, A. Wallraff, S. M. Girvin, and R. J. Schoelkopf, Cavity quantum electrodynamics for superconducting electrical circuits: An architecture for quantum computation, *Phys. Rev. A* **69**, 062320 (2004).
 - [8] A. Wallraff, D. I. Schuster, A. Blais, L. Frunzio, R.-S. Huang, J. Majer, S. Kumar, S. M. Girvin, and R. J. Schoelkopf, Strong coupling of a single photon to a superconducting qubit using circuit quantum electrodynamics, *Nature* **431**, 162 (2004).
 - [9] H. J. Kimble, Strong interactions of single atoms and photons in cavity qed, *Physica Scripta* **1998**, 127 (1998).
 - [10] K. Hammerer, A. S. Sørensen, and E. S. Polzik, Quantum interface between light and atomic ensembles, *Rev. Mod. Phys.* **82**, 1041 (2010).
 - [11] H. J. Kimble, The quantum internet, *Nature* **453**, 1023 (2008).
 - [12] F. V. Gubarev, I. V. Dyakonov, M. Y. Saygin, G. I. Struchalin, S. S. Straupe, and S. P. Kulik, Improved heralded schemes to generate entangled states from single photons, *Phys. Rev. A* **102**, 012604 (2020).
 - [13] S. A. Fldzhyan, M. Y. Saygin, and S. P. Kulik, Compact linear optical scheme for bell state generation, *Phys. Rev. Res.* **3**, 043031 (2021).
 - [14] M. Piccolini, V. Giovannetti, and R. Lo Franco, Asymptotically deterministic robust preparation of maximally entangled bosonic states, *Phys. Rev. Res.* **6**, 013073 (2024).
 - [15] D. B. Uskov, L. Kaplan, A. M. Smith, S. D. Huver, and J. P. Dowling, Maximal success probabilities of linear-optical quantum gates, *Phys. Rev. A* **79**, 042326 (2009).
 - [16] F. Li, M. Yuan, Z. Wang, C. Zhong, and L. Jiang, Enhancing microwave-optical bell pairs generation for quantum transduction using kerr nonlinearity (2025), arXiv:2505.00824 [quant-ph].
 - [17] M. Ohliger, K. Kieling, and J. Eisert, Limitations of quantum computing with gaussian cluster states, *Phys. Rev. A* **82**, 042336 (2010).
 - [18] C. Weedbrook, S. Pirandola, R. García-Patrón, N. J. Cerf, T. C. Ralph, J. H. Shapiro, and S. Lloyd, Gaussian quantum information, *Rev. Mod. Phys.* **84**, 621 (2012).
 - [19] A. S. Parkins, E. Solano, and J. I. Cirac, Unconditional two-mode squeezing of separated atomic ensembles, *Phys. Rev. Lett.* **96**, 053602 (2006).
 - [20] F. Xue, Y.-x. Liu, C. P. Sun, and F. Nori, Two-mode squeezed states and entangled states of two mechanical resonators, *Phys. Rev. B* **76**, 064305 (2007).
 - [21] S. Kotler, G. A. Peterson, E. Shojaei, F. Lecocq, K. Cicak, A. Kwiatkowski, S. Geller, S. Glancy, E. Knill, R. W. Simmonds, J. Aumentado, and J. D. Teufel, Direct observation of deterministic macroscopic entanglement, *Science* **372**, 622 (2021).
 - [22] T. A. Palomaki, J. D. Teufel, R. W. Simmonds, and K. W. Lehnert, Entangling mechanical motion with microwave fields, *Science* **342**, 710 (2013).
 - [23] W. S. Leong, M. Xin, Z. Chen, Y. Wang, and S.-Y. Lan, Creation of two-mode squeezed states in atomic mechanical oscillators, *Phys. Rev. Lett.* **131**, 193601 (2023).
 - [24] C. Eichler, D. Bozyigit, C. Lang, M. Baur, L. Steffen, J. M. Fink, S. Filipp, and A. Wallraff, Observation of two-mode squeezing in the microwave frequency domain, *Phys. Rev. Lett.* **107**, 113601 (2011).
 - [25] B. Abdo, W. Shanks, O. Jinka, J. R. Rozen, and J. Orcutt, Teleportation and entanglement swapping of continuous quantum variables of microwave radiation, *Phys. Rev. X* **15**, 031075 (2025).
 - [26] P.-T. Fong, S. C. Poon, and H.-K. Lau, Characterization and optimized engineering of bosonic quantum interfaces under single-mode operational constraints, *Phys. Rev. Res.* **6**, 013204 (2024).
 - [27] S. L. Braunstein and H. J. Kimble, Teleportation of continuous quantum variables, *Phys. Rev. Lett.* **80**, 869 (1998).
 - [28] J. Eisert, S. Scheel, and M. B. Plenio, Distilling gaussian states with gaussian operations is impossible, *Phys. Rev. Lett.* **89**, 137903 (2002).
 - [29] J. Niset, J. Fiurášek, and N. J. Cerf, No-go theorem for gaussian quantum error correction, *Phys. Rev. Lett.* **102**, 120501 (2009).
 - [30] M. Ohliger, K. Kieling, and J. Eisert, Limitations of quantum computing with gaussian cluster states, *Phys. Rev. A* **82**, 042336 (2010).
 - [31] H. Krovi, S. Guha, Z. Dutton, J. A. Slater, C. Simon, and W. Tittel, Practical quantum repeaters with parametric down-conversion sources, *Applied Physics B* **122**, 52 (2016).
 - [32] P. Dhara, S. J. Johnson, C. N. Gagatsos, P. G. Kwiat, and S. Guha, Heralded multiplexed high-efficiency cascaded source of dual-rail entangled photon pairs using spontaneous parametric down-conversion, *Phys. Rev. Appl.* **17**, 034071 (2022).
 - [33] S. Daffer and P. L. Knight, Generating optimal states for a homodyne bell test, *Phys. Rev. A* **72**, 034101 (2005).
 - [34] A. Tipsmark, J. S. Neergaard-Nielsen, and U. L. Andersen, Displacement-enhanced entanglement distillation of single-mode-squeezed entangled states, *Opt. Express* **21**, 6670 (2013).
 - [35] S.-Y. Lee, S.-W. Ji, H.-J. Kim, and H. Nha, Enhancing quantum entanglement for continuous variables by a coherent superposition of photon subtraction and addition, *Phys. Rev. A* **84**, 012302 (2011).
 - [36] W. SON, M. S. KIM, J. LEE, and D. AHN, Entanglement transfer from continuous variables to qubits, *Journal of Modern Optics* **49**, 1739 (2002).
 - [37] F. Casagrande, A. Lulli, and M. G. A. Paris, Improving the entanglement transfer from continuous-variable systems to localized qubits using non-gaussian states, *Phys. Rev. A* **75**, 032336 (2007).
 - [38] M. Paternostro, G. Falci, M. Kim, and G. Massimo Palma, Entanglement between two superconducting qubits via interaction with nonclassical radiation, *Phys. Rev. B* **69**, 214502 (2004).
 - [39] C. Navarrete-Benlloch, R. García-Patrón, J. H.

- Shapiro, and N. J. Cerf, Enhancing quantum entanglement by photon addition and subtraction, *Phys. Rev. A* **86**, 012328 (2012).
- [40] M. S. Winnel, N. Hosseinidehaj, and T. C. Ralph, Generalized quantum scissors for noiseless linear amplification, *Phys. Rev. A* **102**, 063715 (2020).
- [41] Z. Han and H.-K. Lau, Downloading many-qubit entanglement from continuous-variable cluster states, *Phys. Rev. Lett.* **136**, 040202 (2026).
- [42] M. A. Nielsen, Conditions for a class of entanglement transformations, *Phys. Rev. Lett.* **83**, 436 (1999).
- [43] G. Vidal, Entanglement of pure states for a single copy, *Phys. Rev. Lett.* **83**, 1046 (1999).
- [44] G. Giedke, J. Eisert, J. I. Cirac, and M. B. Plenio, Entanglement transformations of pure gaussian states (2003), arXiv:quant-ph/0301038 [quant-ph].
- [45] C. H. Bennett, H. J. Bernstein, S. Popescu, and B. Schumacher, Concentrating partial entanglement by local operations, *Phys. Rev. A* **53**, 2046 (1996).
- [46] M. A. Nielsen and I. L. Chuang, *Quantum Computation and Quantum Information* (Cambridge University Press, Cambridge, 2010).
- [47] L. Hardy, Method of areas for manipulating the entanglement properties of one copy of a two-particle pure entangled state, *Phys. Rev. A* **60**, 1912 (1999).
- [48] J. G. Jensen and R. Schack, Simple algorithm for local conversion of pure states, *Phys. Rev. A* **63**, 062303 (2001).
- [49] E. Andersson and D. K. L. Oi, Binary search trees for generalized measurements, *Phys. Rev. A* **77**, 052104 (2008).
- [50] G. H. Hardy, J. E. Littlewood, and G. Pólya, *Inequalities* (Cambridge University Press, Cambridge, 1952).
- [51] A. Einstein, B. Podolsky, and N. Rosen, Can quantum-mechanical description of physical reality be considered complete?, *Phys. Rev.* **47**, 777 (1935).
- [52] P. Kok and S. L. Braunstein, Postselected versus nonpostselected quantum teleportation using parametric down-conversion, *Phys. Rev. A* **61**, 042304 (2000).
- [53] J.-W. Pan, Z.-B. Chen, C.-Y. Lu, H. Weinfurter, A. Zeilinger, and M. Żukowski, Multiphoton entanglement and interferometry, *Rev. Mod. Phys.* **84**, 777 (2012).
- [54] J. Brendel, E. Mohler, and W. Martienssen, Time-resolved dual-beam two-photon interferences with high visibility, *Phys. Rev. Lett.* **66**, 1142 (1991).
- [55] G. B. Xavier, J.-Å. Larsson, P. Villoresi, G. Vallone, and A. Cabello, Energy-time and time-bin entanglement: past, present and future, *npj Quantum Information* **11**, 129 (2025).
- [56] C. Simon, H. de Riedmatten, M. Afzelius, N. Sangouard, H. Zbinden, and N. Gisin, Quantum repeaters with photon pair sources and multimode memories, *Phys. Rev. Lett.* **98**, 190503 (2007).
- [57] D. Jonathan and M. B. Plenio, Minimal conditions for local pure-state entanglement manipulation, *Phys. Rev. Lett.* **83**, 1455 (1999).
- [58] M. B. Plenio and S. Virmani, An introduction to entanglement measures, *Quantum Info. Comput.* **7**, 1–51 (2007).
- [59] L. Lewin, *Polylogarithms and Associated Functions* (North Holland, 1981).
- [60] M. Abramowitz and I. A. Stegun, *Handbook of Mathematical Functions*, NBS Applied Mathematical Series, Vol. 55 (National Bureau of Standards, Washington, DC, 1964).
- [61] M. Reck, A. Zeilinger, H. J. Bernstein, and P. Bertani, Experimental realization of any discrete unitary operator, *Phys. Rev. Lett.* **73**, 58 (1994).
- [62] G. Wang and M. Ying, Realization of positive-operator-valued measures by projective measurements without introducing ancillary dimensions (2006), arXiv:quant-ph/0608235 [quant-ph].
- [63] A. Lucas, Ising formulations of many np problems, *Frontiers in Physics* **Volume 2 - 2014**, 10.3389/fphy.2014.00005 (2014).
- [64] C.-H. Wang, K. Noh, J. Lebreuilly, S. Girvin, and L. Jiang, Photon-number-dependent hamiltonian engineering for cavities, *Phys. Rev. Appl.* **15**, 044026 (2021).
- [65] M. Kudra, M. Kervinen, I. Strandberg, S. Ahmed, M. Scigliuzzo, A. Osman, D. P. Lozano, M. O. Tholén, R. Borgani, D. B. Haviland, G. Ferrini, J. Bylander, A. F. Kockum, F. Quijandría, P. Delsing, and S. Gasparinetti, Robust preparation of wigner-negative states with optimized snap-displacement sequences, *PRX Quantum* **3**, 030301 (2022).
- [66] J. Landgraf, C. Flühmann, T. Fösel, F. Marquardt, and R. J. Schoelkopf, Fast quantum control of cavities using an improved protocol without coherent errors, *Phys. Rev. Lett.* **133**, 260802 (2024).
- [67] P.-T. Fong and H.-K. Lau, Engineering non-gaussian bosonic gates through quantum signal processing (2025), arXiv:2508.20261 [quant-ph].